



CrossMark
click for updates

Cite this: *RSC Adv.*, 2015, 5, 8397

Application of 2D-MoO₃ nano-flakes in organic light emitting diodes: effect of semiconductor to metal transition with irradiation†

Janardan Dagar,^{*a} Priyanka Tyagi,^{ab} Razi Ahmad,^a Rashmi Singh,^c O. P. Sinha,^c C. K. Suman^a and Ritu Srivastava^{*a}

The current work demonstrates efficient utilization of 2D-MoO₃ nano-flakes as a hole injection layer (HIL) in organic light emitting diodes (OLEDs). Nano-flakes are synthesized using an organic solvent-assisted grinding and sonication method of liquid exfoliation for MoO₃, and 8–16 nm thick flakes are obtained. The effect of solar illumination on the hole injection properties of these nano-flakes is then studied by exposing the nano-flakes for 0, 15, 30, 45, 60 and 120 min and using them as HIL in green OLED. The device results are then compared with the OLED having bulk MoO₃ as HIL. OLEDs with nano-flakes as the HIL have shown better performance than the OLED with bulk MoO₃ as the HIL due to the better semiconducting properties in the nano-flake phase. The luminous intensity is increased by increasing the duration of irradiation and was found to be optimum in case of nano-flakes irradiated for 30 or 45 min and then started to decrease with the increase of duration of irradiation. The current density in the OLEDs with nano-flakes as the HIL shows a switching from high resistance to low resistance; however, the sequential pattern of switching voltage was missing with the duration of irradiation. The current density also decreased for nano-flakes with 60 and 120 min of irradiation. Transition from the semiconducting to metal nature of nano-flakes by solar irradiation is suggested to be the reason behind this decrease in current density and luminous intensity with a longer duration of illumination.

Received 15th October 2014
Accepted 15th December 2014

DOI: 10.1039/c4ra12430h

www.rsc.org/advances

Introduction

Two dimensional (2D) nanostructures exhibit superior crystalline, optical and electronic properties in comparison to bulk materials.^{1–6} Graphene is one of the most widely investigated examples of 2D nanostructures and by far remains a preferred choice as an ideal 2D material.^{2,7–10} However, the absence of band gap in graphene 2D sheets has limited its application, and alternative 2D materials are required.^{11–17} Recent advances in the field of synthesis led to the realization of 2D metal oxide nano-structures, which by default possess an optical band gap, leading to interesting optical properties.^{1,3,4,6} Stable 2D semiconducting oxide of tungsten and molybdenum has been investigated widely and utilized for sensing, field emission and several other applications.^{18–25}

MoO₃ 2D nano-flakes are found to be of particular interest due to their potential applications. MoO₃ nano-flakes have been used for hydrogen gas (H₂) sensing, photoluminescence and field emission.^{24–26} Recently, Alsaif *et al.*²⁷ demonstrated tunable plasmon resonances from 2D MoO₃ nano-flakes. These reports have shown the potential of MoO₃ nano-flakes; however, their application in devices is required to further prove their potential. Bulk MoO₃ has been successfully used in organic electronic devices such as organic light emitting diodes (OLEDs) and organic photovoltaics as a hole injection and extraction layer, where the semiconducting properties of MoO₃ has improved the efficiencies of these devices significantly.^{28–34} Moving from bulk to 2D nano-flakes is expected to improve the crystalline structure of MoO₃, which thereby is expected to improve the semiconducting properties. This has motivated us to utilize the 2D MoO₃ nano-flakes as the hole injection layer (HIL) in OLEDs.

Several methods for the synthesis and fabrication of 2D MoO₃ nano-flakes have been reported in recent years. The most successful methods are the modified hot plate method,²⁵ the plasma assisted paste sublimation process,³⁵ the organic solvent assisted grinding and sonication method,^{26,27} *etc.* Here, we adapted the organic solvent-assisted grinding and sonication method of liquid exfoliation to bulk MoO₃ to obtain 2D nano-flakes. Alsaif *et al.*²⁷ observed that the controlled solar illumination of a 2D MoO₃ nano-flake suspension alters its

^aCSIR-Network of institute for solar energy (NISE), Physics of Energy Harvesting Division, CSIR-National Physical Laboratory, Dr K.S.Krishnan Road, New Delhi-110012, India. E-mail: ritu@mail.nplindia.org; j.dagarccet@gmail.com; Fax: +91-11-45609310; Tel: +91-11-45608644

^bCenter for Applied Research in Electronics, Indian Institute of Technology Delhi, New Delhi-110016, India

^cAmity Institute of Nanotechnology, Amity University, Noida, U.P., India

† Electronic supplementary information (ESI) available. See DOI: 10.1039/c4ra12430h

properties drastically, according to characterizations by Raman, X-ray diffraction, and X-ray photoelectron spectroscopy (XPS). They observed that the solar illumination of these nano-flakes decreases the semiconducting properties and induces metallic properties as the duration of exposure is increased. Here, to observe the effect of solar illumination on the properties of 2D MoO₃ nano-flakes, OLEDs with nano-flakes as the HIL exposed for different durations have been fabricated and their effects on device characteristics are discussed.

Experimental

Synthesis of nano-flakes

Molybdenum trioxide (99.99%) powder (Sigma-Aldrich) was used for the synthesis of 2D nano-flakes using the method previously reported.^{26,27} Nano-flakes were prepared using organic solvent assisted grinding in which 1 g of MoO₃ powder was ground with 0.2 ml acetonitrile for 1 h. The resultant powder was then dispersed in a 15 ml mixture of ethanol and water in 1 : 1 composition and sonicated for 3 h. The solution was then centrifuged at 6000 rpm for 45 min at room temperature, and a light yellow/blue supernatant liquid was collected that contained a high concentration of 2D MoO₃ nano-flakes. The supernatant solution was distributed in six Agilent sample tubes and then irradiated with a homemade solar simulator at 100 mW cm⁻² power for different time durations of 15 min, 30 min, 45 min, 60 min and 120 min.

Characterization of nano-flakes

2D MoO₃ nano-flakes were characterized according to their surface morphology, absorption spectra and Raman spectra. Surface morphology was studied using atomic force microscopy (AFM; NTMDT Solvar Pro P47). Morphological measurements were performed for the nano-flakes spin coated on indium tin oxide (ITO) coated glass substrates. The UV-Vis absorption spectrum was recorded in solution form using a Shimadzu UV-Vis spectrophotometer, model no. UV-2401 PV. The Raman spectra were acquired using a Renishaw inVia Reflex Raman spectrometer, UK, with an excitation source of 514.5 nm and 2.5 mW power.

Device fabrication

OLEDs were fabricated on ITO coated glass substrates having a sheet resistance of 20 Ω □⁻¹ and a thickness of 120 nm. Substrates were first cleaned using deionized water, acetone, trichloroethylene and isopropyl alcohol for 20 min each using an ultrasonic bath and dried in vacuum oven. Prior to the deposition of organic layers, 2D nano-flakes were repeatedly spin coated twice on the cleaned ITO coated substrate at 2000 rpm for 1 minute and then dried at 120 °C temperature for 1 hour. The device structure was ITO (120 nm)/α-NPD (35 nm)/5% Ir(ppy)₃ doped CBP (30 nm)/BCP (6 nm)/Alq₃ (28 nm)/LiF (1 nm)/Al (150 nm). Tris (8-hydroxyquinoline) aluminium (Alq₃) (Sigma-Aldrich) and *N,N'*-di-[(1-naphthalenyl)-*N,N'*-diphenyl]-(1,1'-biphenyl)-4,4'-diamine (α-NPD) (Sigma-Aldrich) were used as the electron and hole

transporting layers. 2,9 Dimethyl 4,7 diphenyl 1,10 phenanthroline (BCP) (Sigma-Aldrich), which has a high ionization potential (6.5 eV), has been used as a hole blocking layer, and lithium fluoride (LiF)/aluminium (Al) and ITO have been used as the cathode and anode, respectively. Organic layers were deposited under a base pressure of 4 × 10⁻⁶ torr at a deposition rate of 2.4 nm min⁻¹. The thickness of the deposited layers was measured *in situ* by a quartz crystal thickness monitor and reconfirmed by variable angle ellipsometry. The size of each pixel was 3 mm × 4 mm. The electroluminescence (EL) spectrum was measured with a high resolution spectrometer (Ocean optics HR-2000 CG UV-NIR). The current density-voltage-luminescence (*J-V-L*) characteristics were measured with a luminance meter (LMT-1009) interfaced with a Keithley 2400 programmable current-voltage digital source meter. All measurements were carried out at room temperature under ambient conditions.

Results and discussion

Fig. 1a shows the optical images of the nano-flake suspension at different solar irradiation conditions. The suspension was initially found to be of light blue color and gradually turned into dark blue upon increase of irradiation time, and the effect of solar radiation was found to be similar to that previously reported.²⁷ As the intended utilization of these nano-flakes is as a HIL in OLEDs, the surface morphology of nano-flakes deposited on ITO coated glass substrates was first characterized using AFM. A high density of nano-flakes is required for their efficient utilization as a HIL in OLEDs. To accomplish a high density, nano-flake solution was repeatedly coated three times on the substrates, and the AFM image is shown in Fig. 1b. The filling fraction of nano-flakes was calculated from the AFM image and found to be ~30%, which was relatively small for one and two layer coating (Fig. S1†).³⁸ Fig. 1c depicts the AFM image for a single flake, also showing the thickness and lateral dimension profile. The thickness of flakes was found to be in the range of 8–16 nm (constituting 20–40 mono-layers), and the lateral dimensions were found to be 60–80 and 80–120 nm, respectively. The thickness dimension of the flakes is found to be nearly 10 times smaller than the lateral dimension; therefore, the flakes can be regarded as 2D flakes.

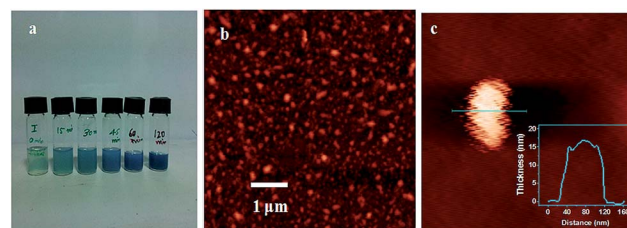


Fig. 1 (a) Optical images of nano-flakes suspension irradiated for different duration of time. (b) AFM image of nano-flakes deposited by three repeated coatings over an ITO coated substrate and used as a HIL in OLEDs. (c) AFM image of single flake showing the thickness and lateral dimensions.

2D-MoO₃ nano-flakes were implemented as the HIL in OLEDs. Green OLEDs were fabricated with MoO₃ nano-flakes prepared using different irradiation times (t_{irr}). Devices were designated as device 1, 2, 3, 4, 5 and 6 for $t_{\text{irr}} = 0, 15, 30, 45, 60$ and 120 min, respectively, and for comparison, a device with bulk MoO₃ as the injection layer was also prepared. Fig. 2 shows the images of the biased OLEDs without HIL, reference device, and devices 1–6. All of the devices were found to be bright and efficient. The luminous intensity of the devices at a current density of 1000 A m⁻² is also mentioned in the figure. It can be seen that the devices with nano-flakes exhibit superior luminous intensity than the device without a HIL and the device with bulk MoO₃ as the HIL. The EL spectrum of OLEDs was found to be unaffected by the use of nano-flakes as the HIL (Fig. S3†).³⁸

Fig. 3 depicts the V - L characteristics for these devices. The device with the bulk MoO₃ interface layer and Device 1 have nearly same values of luminous intensity over the entire voltage range. This indicates that the device with 2D-MoO₃ nano-flakes has the same effect on the luminescence as bulk MoO₃. As the 2D-MoO₃ nano-flakes were irradiated and used in device 2, the luminous intensity has increased significantly. The increase in luminescence is nearly 1.3–1.4 times that of device 1. Further, device 3 with 2D-MoO₃ nano-flakes with $t_{\text{irr}} = 30$ min as the HIL has a higher luminous intensity in comparison to device 2, and the increase in luminous intensity is about 1.6–1.7 times that for device 1 over the entire region of voltage. The luminous intensity is then saturated with 2D-MoO₃ nano-flakes with $t_{\text{irr}} = 45$ min for device 4. 2D-MoO₃ nano-flakes with increased t_{irr} to 60 and 120 min led to a decrease in luminous intensity in devices 5 and 6 and the luminous intensity became almost equal to that of the device with a bulk MoO₃ layer. These results indicate that the device characteristics with 2D-MoO₃ nano-flakes as the interface layer strongly depend on the duration of irradiation.

For the complete analysis of device characteristics, J - V characteristics were also measured for these devices and are depicted in Fig. 4. Unlike the L - V characteristics, the device with bulk MoO₃ layer possesses a higher current density in comparison to the other devices. Also, as the bulk MoO₃ is

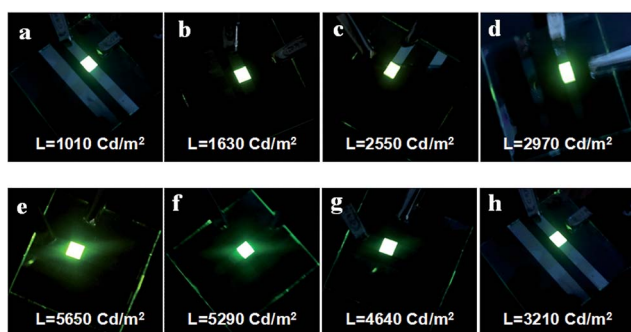


Fig. 2 Images of biased OLEDs (at an operating current density of 1000 A m⁻²) (a) without HIL, (b) with bulk MoO₃ as HIL and with nano-flakes as HIL, where pictures (c–h) correspond to the irradiation times of 0, 15, 30, 45, 60 and 120 min, respectively. Values of luminous intensity at 1000 A m⁻² are also included in each image.

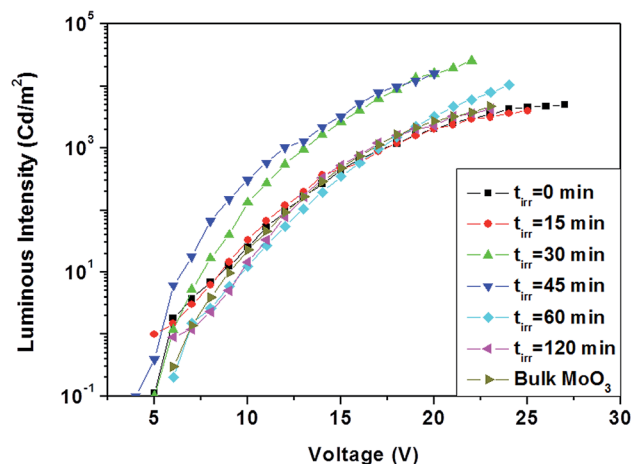


Fig. 3 Luminescence–voltage characteristics for OLEDs with 2D-MoO₃ nano-flakes as the hole injection layer with different durations of irradiation. Data for OLED with bulk MoO₃ are also included.

replaced by the 2D-MoO₃ nano-flakes without irradiation, the current density is decreased by almost one order of magnitude in the high voltage region ($V > 15$ V). For $V < 11$ V, the current density is almost equal to the current density of the device with bulk MoO₃. This indicates that the total resistance of the device is lower in the low voltage region and increased in the high voltage region.

One interesting fact to be noted is that this increase in resistance has no effect on the luminous intensity, as can be seen from Fig. 3. A similar pattern has also been observed in device 2, where the total resistance of the device switched from a high value to a low value after 9 V. Similar to that for device 1, this switching has not affected the luminous intensity of the device. Device 2 has a higher ratio of high resistance to low resistance values. As the t_{irr} is increased to 30 and 45 min in devices 3 and 4, this switching from the high resistance to low

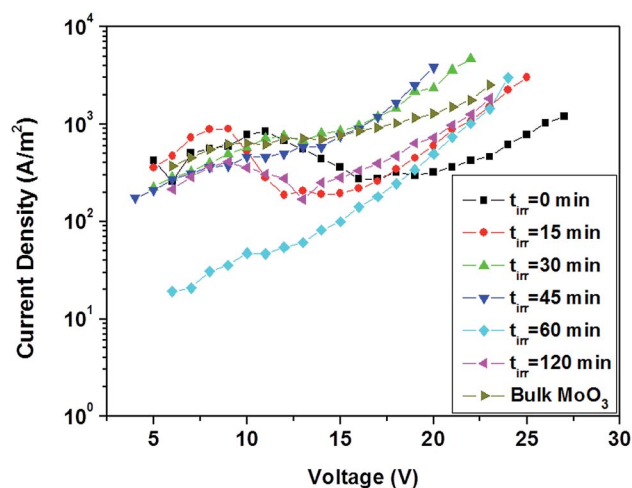


Fig. 4 Current density–voltage characteristics for OLEDs with 2D-MoO₃ nano-flakes as the hole injection layer with different durations of irradiation. Data for OLED with bulk MoO₃ are also included.

resistance region disappears, and also the current density values are highest for these two devices for voltages higher than 15 V. Further increases in the t_{irr} in devices 5 and 6 decreased the current density significantly. It is evident from the luminous intensity data that even the total device resistance varies among devices 1–6, and all the devices have similar or better luminous intensities in comparison to the reference device with bulk MoO₃ as the interface layer. This strongly suggests the improved hole injection properties of nano-flakes in comparison to bulk MoO₃.

Fig. 5 depicts the J – L characteristics for these devices in order to provide a clearer picture of the device results. It is evident from the figure that all devices with 2D-MoO₃ nano-flakes have a higher ratio of luminous intensity–current density in comparison to the device with bulk MoO₃ interface layer. The slope of J – L characteristics represent the current efficiency of the device, and it can be seen from the figure that it has increased in the case of device 1 in comparison to the reference device. However, the efficiency started to decrease in the high current density region, where the luminous intensity is almost invariant with the increase in voltage. Device 2 possesses a higher efficiency in comparison to device 1 in the low current density region, while it follows the same pattern in the high voltage region. Devices 3 and 4 have a slightly lower efficiency in comparison to devices 1 and 2; however, the efficiency remains invariant in these devices with changes in current density. Devices 5 and 6 have shown relatively lower efficiency in comparison to devices 1–4 in the whole current density region. The highest efficiency has been achieved in the cases of device 1, 2, 3 and 4. Combining the results for the V – L , J – V and J – L characteristics, it can be concluded that devices with 2D-MoO₃ nano-flakes show superior performance in comparison to the device with bulk MoO₃, and the device efficiency is dependent on the irradiation time. Device 4 can be considered optimum in terms of current density and luminous intensity.

For further quantification of the device performance, the current efficiency is plotted as a function of voltage in Fig. 6. It can be seen from the figure that devices with nano-flakes exhibit better performance than the device with bulk MoO₃ as the HIL. At 15 V, the current efficiency has increased with nano-flakes in comparison to the bulk MoO₃, and it further increases with the duration of irradiation of up to 45 min when it starts to decrease. The current efficiency is highest for the 45 min duration of irradiation.

These observations can be explained on the basis of the reported transition of 2D-MoO₃ nano-flakes from semiconductor to metal phase upon increasing the duration of irradiation.²⁷ The starting material in the preparation of nano-flakes is α -MoO₃, which is an n-type semiconductor and thus acts as an efficient HIL at the ITO/HTL interface. 2D-MoO₃ nano-flakes possess a more crystalline form of α -MoO₃ in comparison to bulk MoO₃.^{25,27} Therefore, it serves as a better HIL in comparison to bulk MoO₃. As the chemically synthesized nano-flakes are irradiated, the injection properties increase, which is indicative of the better semiconductor behavior of α -MoO₃. To confirm this, we have measured the Raman spectra of 2D-MoO₃ nano-flakes without irradiation and with $t_{\text{irr}} = 15$ min. Fig. 7 shows the Raman spectra for these nano-flakes coated on Si substrates. Raman peaks of Si have been filtered in this figure for better observation. It can be seen from the figure that Raman peaks have higher intensities (at 304, 427, 617 and 671 cm⁻¹) for irradiated nano-flakes. Fig. 7 also shows the Raman spectra of MoO₃ nano-flakes with $t_{\text{irr}} = 120$ min and clearly shows that all the peak intensities are reduced significantly in this film. This may be the reason behind the decrease in efficiency for devices 5 and 6, for which increased irradiation reduced the semiconducting properties of nano-flakes. It has been observed by Alsaif *et al.*²⁶ that the irradiation of α -MoO₃ causes formation of the Mo⁵⁺ oxidation state by a possible reduction of MoO₃ to Mo₄O₁₁. Mo⁵⁺ has a lower binding energy in comparison to Mo⁶⁺ (formed in case of MoO₃) and therefore

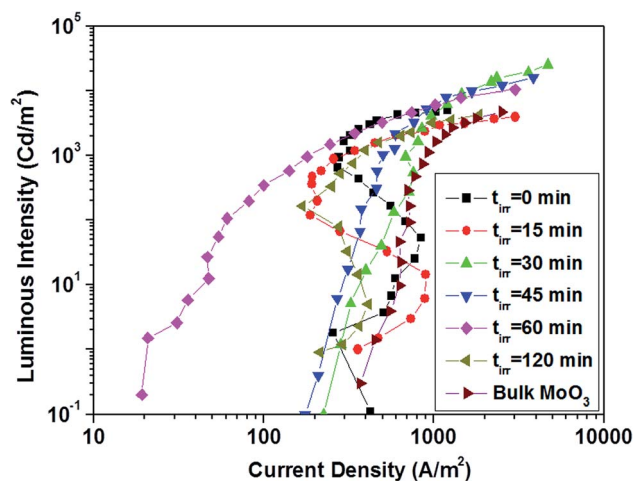


Fig. 5 Current density–luminous intensity characteristics for devices 1, 2, 3, 4, 5 and 6 with 2D-MoO₃ nano-flakes irradiated for 0, 15, 30, 45, 60 and 120 min as the hole injection layer. For reference, data for bulk MoO₃ as the HIL are also included.

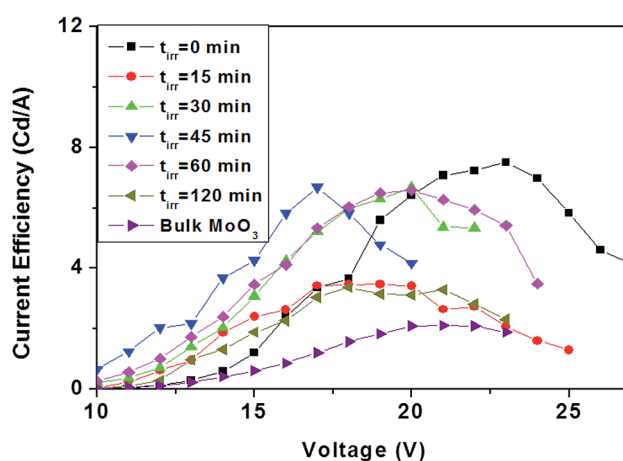


Fig. 6 Current efficiency–voltage characteristics for devices 1, 2, 3, 4, 5 and 6 with 2D-MoO₃ nano-flakes irradiated for 0, 15, 30, 45, 60 and 120 min as the hole injection layer. For reference, data for bulk MoO₃ as the HIL are also included.

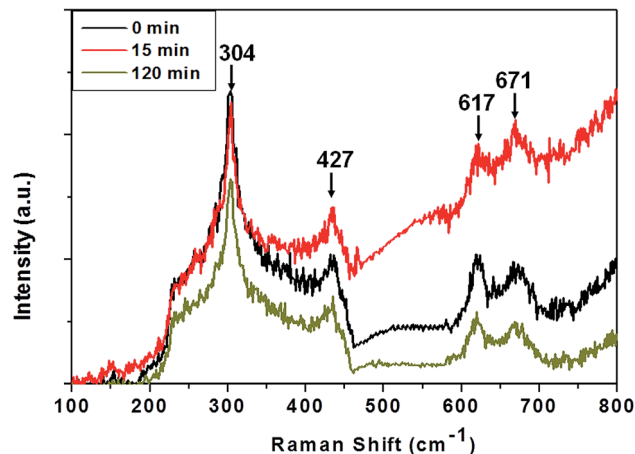


Fig. 7 Raman spectra for 2D-MoO₃ nano-flakes irradiated for 0, 15 and 120 min duration and deposited on Si substrates. For clear observation, the peak due to Si is filtered.

represents the metallic state. It was also been observed by the authors by X-ray photoelectron spectroscopy (XPS) that the intensity of Mo⁵⁺ increases and that of Mo⁶⁺ decreases with an increase in the duration of irradiation. The metallic state of 2D-MoO₃ nano-flakes will therefore act as charge trapping center at the ITO/HTL interface, similar to the case reported for gold nano-particles used in polymer OLEDs.^{36,37} This trapping and de-trapping of charge carrier may be the reason for switching from low to high resistance regions in devices with nano-flakes. However, the switching has not been found to follow any specific pattern in our devices, which could be due to the low coverage of 2D-MoO₃ nano-flakes.

It has also been observed by Alsaif *et al.*²⁷ that upon irradiation, MoO₃ nano-flakes start to possess localized surface plasmon resonance (LSPR) identified as an absorption peak in near infra-red (NIR) region. This peak was found to be dependent on the duration of irradiation. Therefore, the UV-Vis spectra were measured for the 2D MoO₃ nano-flakes with

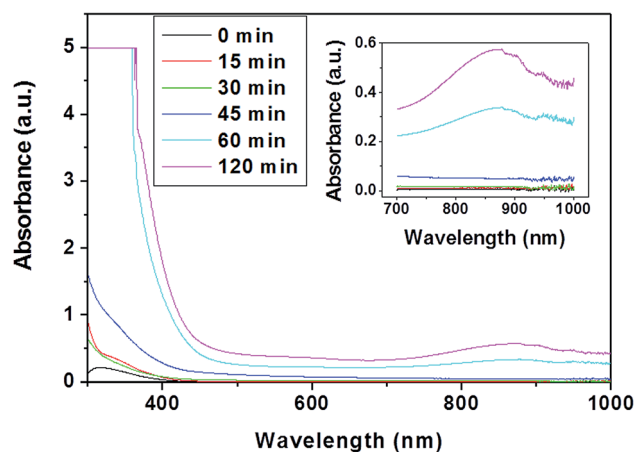


Fig. 8 UV-Vis spectra recorded for 2D MoO₃ nano-flakes irradiated for 0, 15, 30, 45, 60 and 120 min. Inset shows the magnified view of the NIR region.

different t_{irr} in solution form as depicted in Fig. 8. The inset of this figure shows the magnified view of the NIR region (the region of interest). It is evident from this figure that for the 60 and 120 min durations of exposure, the 2D MoO₃ nano-flakes start to show the LSPR peaks in the NIR region. This supports our device results in which the current density decreases for the 2D MoO₃ nano-flakes having a t_{irr} of 60 and 120 min. However, our UV-Vis spectra were found to be a little different from those observed by Alsaif *et al.*²⁷ In their results, they started to see LSPR with 5 min exposure of nano-flakes. The reason behind this discrepancy may be the different experimental conditions and different size of nano-flakes.

Further, we have also measured the work function of 2D-MoO₃ nano-flakes ($t_{\text{irr}} = 120$ min) deposited on ITO coated glass substrates by surface Kelvin probe microscopy using a gold tip, and the observed signals are shown in Fig. S2(a) and (b).^{†38} The work function has decreased upon deposition of nano-flakes with $t_{\text{irr}} = 120$ min, which further explains the device results and justifies the decrease in current in the case of device 6. Generally, semiconducting MoO₃ increased the work function of ITO; however, for higher irradiation times, MoO₃ nano-flakes have acquired a metallic state, which could lead to a reduction of work function because the metallic form of Mo has lower value of surface potential in comparison to ITO. The decrease in work function was found to be nearly 160 meV, which resulted in a higher interface resistance for nano-flakes with a higher duration of irradiation. When nano-flakes are used in place of bulk MoO₃, the current efficiency of the device is increased from 0.6 to 1.22 Cd A⁻¹ at 15 V, which is expected due to the improved semiconducting nature in the nano-phase. As the irradiated nano-flakes are used, the current efficiency is further increased to 2.36, 3.05 and 4.3 Cd A⁻¹ for 15, 30 and 45 min of irradiation, respectively. The increasing pattern of current efficiency with duration of irradiation is a signature of the improved semiconducting nature of nano-flakes with irradiation as already discussed with the help of Raman spectra. A further increase in the irradiation duration to 60 and 120 min transforms the nano-flakes into metallic form as depicted from the LSPR peaks observed in Fig. 8. The metallic nature of nano-flakes reduces the work function of ITO as measured by Kelvin probe and therefore deteriorates the injection properties. This leads to a decrease in current efficiency to 3.42 and 2 Cd A⁻¹ for 60 and 120 min irradiated nano-flakes, respectively. Therefore, the effect of transition from semiconducting to metallic nature of nano-flakes is clearly observed in the devices.

In conclusion, the current work demonstrates the use of 2D MoO₃ nano-flakes as an efficient HIL for OLEDs. Nano-flakes irradiated for 0, 15, 30, 45, 60 and 120 min with solar power were used for this study, and the device results with nano-flakes as the HIL were compared with that with bulk MoO₃ as the HIL. OLEDs with nano-flakes irradiated for 0, 15, 30 and 45 min were found to be superior in terms of current density and luminescence, and those with nano-flakes irradiated for 60 and 120 min were inferior. Nano-flakes possess better semiconducting properties than bulk MoO₃, which is demonstrated also by the Raman spectra of irradiated nano-flakes. It has been observed that the semiconducting properties of nano-flakes is increased

by irradiation up to 45 min, and then nano-flakes start to possess more metallic properties. This has also been identified by a LSPR peak, which started to appear for nano-flakes with 60 min irradiation time and became stronger when nano-flakes were irradiated for 120 min. The work function of ITO modified by nano-flakes irradiated for 120 min was measured using Kelvin probe microscopy, and it was found to be lower by 0.16 eV in comparison to that of bare ITO. This decrease in work function by MoO₃ nano-flakes irradiated for 60 and 120 min leads to a decrease in current density.

Acknowledgements

The authors gratefully recognize financial support from the project NWP-55 (CSIR-TAPSUN). The authors are also thankful to Dr Bhanu Pratap Singh and Dr Govind for their help in characterization.

References

- 1 R. Mas-Ballesté, C. Gómez-Navarro, J. Gómez-Herrero and F. Zamora, 2D materials: to Graphene and Beyond, *Nanoscale*, 2011, **3**, 20–30.
- 2 A. K. Geim and K. S. Novoselov, The Rise of Graphene, *Nat. Mater.*, 2007, **6**, 183–191.
- 3 M. Xu, T. Liang, M. Shi and H. Chen, Graphene-Like Two-Dimensional Materials, *Chem. Rev.*, 2013, **113**, 3766–3798.
- 4 S. Balendhran, S. Walia, H. Nili, J. Z. Ou, S. Zhuiykov, R. B. Kaner, S. Sriram, M. Bhaskaran and K. Kalantar-zadeh, Two-Dimensional Molybdenum Trioxide and Dichalcogenides, *Adv. Funct. Mater.*, 2013, **23**, 3952–3970.
- 5 N. J. Roome and J. D. Carey, Beyond Graphene: Stable Elemental Monolayers of Silicene and Germanene, *ACS Appl. Mater. Interfaces*, 2014, **6**, 7743–7750.
- 6 Q. H. Wang, K. Kalantar-Zadeh, A. Kis, J. N. Coleman and M. S. Strano, Electronics and Optoelectronics of Two-Dimensional Transition Metal Dichalcogenides, *Nat. Nanotechnol.*, 2012, **7**, 699–712.
- 7 Y. M. Liu, C. Punckt, M. A. Pope, A. Gelperin and I. A. Aksay, Electrochemical Sensing of Nitric Oxide with Functionalized Graphene Electrodes, *ACS Appl. Mater. Interfaces*, 2013, **5**, 12624–12630.
- 8 X. Wang, W. Xie, J. Chen and J.-B. Xu, Homo- and Hetero- p-n Junctions Formed on Graphene Steps, *ACS Appl. Mater. Interfaces*, 2014, **6**, 3–8.
- 9 L. Feng, Z. Zhang, J. Ren and X. Qu, Graphene Platform Used for Electrochemically Discriminating DNA Triplex, *ACS Appl. Mater. Interfaces*, 2014, **6**, 3513–3519.
- 10 J. Sun, H. Zhang, L.-H. Guo and L. Zhao, Two-Dimensional Interface Engineering of a Titania–Graphene Nanosheet Composite for Improved Photocatalytic Activity, *ACS Appl. Mater. Interfaces*, 2013, **5**, 13035–13041.
- 11 Y. Zhang, T.-T. Tang, C. Girit, Z. Hao, M. C. Martin, A. Zettl, M. F. Crommie, Y. R. Shen and F. Wang, Direct Observation of a Widely Tunable Bandgap in Bilayer Graphene, *Nature*, 2009, **459**, 820–823.
- 12 E. V. Castro, K. S. Novoselov, S. V. Morozov, N. M. R. Peres, J. M. B. Lopes dos Santos, J. Nilsson, F. Guinea, A. K. Geim and A. H. Castro Neto, Biased Bilayer Graphene: Semiconductor with a Gap Tunable by the Electric Field Effect, *Phys. Rev. Lett.*, 2007, **99**, 216802.
- 13 H. Z. Ni, T. Yu, Y. H. Lu, Y. Y. Wang, Y. P. Feng and Z. X. Shen, Uniaxial Strain on Graphene: Raman Spectroscopy Study and Band-Gap Opening, *ACS Nano*, 2008, **2**, 2301–2305.
- 14 J. B. Oostinga, H. B. Heersche, X. Liu, A. F. Morpurgo and L. M. K. Vandersypen, Gate-Induced Insulating State in Bilayer Graphene Devices, *Nat. Mater.*, 2007, **7**, 151–157.
- 15 H. Min, B. Sahu, S. K. Banerjee and A. H. MacDonald, Ab Initio Theory of Gate Induced Gaps in Graphene Bilayers, *Phys. Rev. B: Condens. Matter Mater. Phys.*, 2007, **75**, 155115.
- 16 Z. Luo, P. M. Vora, E. J. Mele, A. T. Charlie Johnson and J. M. Kikkawa, Photoluminescence and Band Gap Modulation in Graphene Oxide, *Appl. Phys. Lett.*, 2009, **94**, 111909.
- 17 K. F. Mak, C. H. Lui, J. Shan and T. F. Heinz, Observation of an Electric-Field-Induced Band Gap in Bilayer Graphene by Infrared Spectroscopy, *Phys. Rev. Lett.*, 2009, **102**, 256405.
- 18 K. Kalantar-zadeh, J. Tang, M. Wang, K. L. Wang, A. Shailos, K. Galatsis, R. Kojima, V. Strong, A. Lech, W. Wlodarski and R. B. Kaner, Synthesis of Nanometre-Thick MoO₃ Sheets, *Nanoscale*, 2010, **2**, 429–433.
- 19 K. Kalantar-zadeh, A. Vijayaraghavan, M.-H. Ham, H. Zheng, M. Breedon and M. S. Strano, Synthesis of Atomically Thin WO₃ Sheets from Hydrated Tungsten Trioxide, *Chem. Mater.*, 2010, **22**, 5660–5666.
- 20 G. Wang, Y. Ling, H. Wang, X. Yang, C. Wang, J. Z. Zhang and Y. Li, Hydrogen-Treated WO₃ Nanoflakes Show Enhanced Photostability, *Energy Environ. Sci.*, 2012, **5**, 6180–6187.
- 21 S. Zhuiykov and E. Kats, Enhanced Electrical Properties in Sub-10 nm WO₃ Nanoflakes Prepared via a Two-Step Sol-Gel-Exfoliation Method, *Nanoscale Res. Lett.*, 2014, **9**, 401.
- 22 Y. Zhao, J. He, M. Yang, S. Gao, G. Zuo, C. Yan and Z. Cheng, Single Crystal WO₃ Nanoflakes as Quartz Crystal Microbalance Sensing Layer for Ultrafast Detection of Trace Sarin Simulant, *Anal. Chim. Acta*, 2009, **654**, 120–126.
- 23 Y. He and Y. Zhao, Near-Infrared Laser-Induced Photothermal Coloration in WO₃·H₂O Nanoflakes, *J. Phys. Chem. C*, 2008, **112**, 61–68.
- 24 J. Z. Ou, J. L. Campbell, D. Yao, W. Wlodarski and K. Kalantar-zadeh, In Situ Raman Spectroscopy of H₂ Gas Interaction with Layered MoO₃, *J. Phys. Chem. C*, 2011, **115**, 10757–10763.
- 25 B. Yan, Z. Zheng, J. Zhang, H. Gong, Z. Shen, W. Huang and T. Yu, Orientation Controllable Growth of MoO₃ Nanoflakes: Micro-Raman, Field Emission, and Birefringence Properties, *J. Phys. Chem. C*, 2009, **113**, 20259–20263.
- 26 M. M. Y. A. Alsaif, S. Balendhran, M. R. Field, K. Latham, W. Wlodarski, J. Z. Ou and K. Kalantar-zadeh, Two Dimensional α -MoO₃ Nanoflakes Obtained Using Solvent-Assisted Grinding and Sonication Method: Application for H₂ Gas Sensing, *Sens. Actuators, B*, 2014, **192**, 196–204.

- 27 M. M. Y. A. Alsaif, K. Latham, M. R. Field, D. D. Yao, N. V. Medehkar, G. A. Beane, R. B. Kaner, S. P. Russo, J. Z. Ou and K. Kalantar-zadeh, Tunable Plasmon Resonances in Two-Dimensional Molybdenum Oxide Nanoflakes, *Adv. Mater.*, 2014, **26**, 3931–3937.
- 28 H. You, Y. Dai, Z. Zhang and D. Ma, Improved Performances of Organic Light-Emitting Diodes with Metal Oxide as Anode Buffer, *J. Appl. Phys.*, 2007, **101**, 026105.
- 29 T. Matsushima, Y. Kinoshita and H. Murata, Formation of Ohmic Hole Injection by Inserting an Ultrathin Layer of Molybdenum Trioxide Between Indium Tin Oxide and Organic Hole-Transporting Layers, *Appl. Phys. Lett.*, 2007, **91**, 253504.
- 30 Z. B. Wang, M. G. Helander, J. Qiu, Z. W. Liu, M. T. Greiner and Z. H. Lu, Direct Hole Injection in to 4,4'-N,N'-Dicarbazole-Biphenyl: A Simple Pathway to Achieve Efficient Organic Light Emitting Diodes, *J. Appl. Phys.*, 2010, **108**, 024510.
- 31 M. Vasilopoulou, L. C. Palilis, D. G. Georgiadou, S. Kennou, I. Kostis, D. Davazoglou and P. Argitis, Barrierless Hole Injection Through Sub-Bandgap Occupied States in Organic Light Emitting Diodes Using Substoichiometric MoO_x Anode Interfacial Layer, *Appl. Phys. Lett.*, 2012, **100**, 013311.
- 32 F. Wang, X. Qiao, T. Xiong and D. Ma, The Role of Molybdenum Oxide as Anode Interfacial Modification in the Improvement of Efficiency and Stability in Organic Light-Emitting Diodes, *Org. Electron.*, 2008, **9**, 985–993.
- 33 V. Shrotriya, G. Li, Y. Yao, C.-W. Chu and Y. Yang, Transition Metal Oxides as the Buffer Layer for Polymer Photovoltaic Cells, *Appl. Phys. Lett.*, 2006, **88**, 073508.
- 34 D. Y. Kim, J. Subbiah, G. Sarasqueta, F. So, H. Ding, Irfan and Y. Gao, The Effect of Molybdenum Oxide Interlayer on Organic Photovoltaic Cells, *Appl. Phys. Lett.*, 2009, **95**, 093304–3.
- 35 R. K. Sharma and G. B. Reddy, Controlled Growth of Vertically Aligned MoO₃ Nanoflakes by Plasma Assisted Paste Sublimation Process, *J. Appl. Phys.*, 2013, **114**, 184310.
- 36 R. J. Tseng, J. Huang, J. Ouyang, R. B. Kaner and Y. Yang, Polyaniline Nanofiber/Gold Nanoparticle Nonvolatile Memory, *Nano Lett.*, 2005, **5**, 1077–1080.
- 37 A. Prakash, J. Ouyang, J.-L. Lin and Y. Yang, Polymer Memory Device Based on Conjugated Polymer and Gold Nanoparticles, *J. Appl. Phys.*, 2006, **100**, 054309.
- 38 ESI.†